Supplementary Information for

Hypergolic Ionic Liquids: To Be or Not to Be?

Souvick Biswas[1], Kazuumi Fujioka[1], Ivan Antonov[1], Grace L. Rizzo[1], Steven D. Chambreau[2], Stefan Schneider[3], Rui Sun[1*], Ralf I. Kaiser[1*]

[1] Department of Chemistry, University of Hawai'i at Manoa, Honolulu, Hawaii 96822, United States

[2] Jacobs Technology, Inc., Edwards Air Force Base, California 93524, United States

[3] Air Force Research Laboratory, Edwards Air Force Base, California 93524, United States

* Corresponding authors. E-mail: ruisun@hawaii.edu, ralfk@hawaii.edu

S1. Experimental method

S1.1. Ultrasonic levitator apparatus: In the acoustic levitator apparatus used in the present experiment, ultrasonic sound waves with a frequency of 58 kHz are produced by a piezoelectric transducer and they are reflected from a concave plate mounted vertically upwards thus generating a standing wave. The soundwaves produce acoustic radiation pressure, which allows a liquid droplet or a tiny solid particle to levitate slightly below one of the pressure minima of the standing wave.[1-3] The distance between the transducer and reflector is set to 2.5 times the wavelength of the soundwave used in the set up (or 14.8 mm) producing five pressure nodes in total, although only the second and third pressure nodes above the ultrasonic transducer are suitable for levitation. The largest diameter of droplets or particles that can be held steadily while levitated in the present apparatus is approximately 3 mm, whereas the smallest could be as low as 15 μm. Here, the droplets loaded in the pressure nodes before merging were oblate spheroidal shaped and their horizontal and vertical diameters measured in the ranges of 1.8-3.0 mm and 1.0-2.1 mm, respectively.

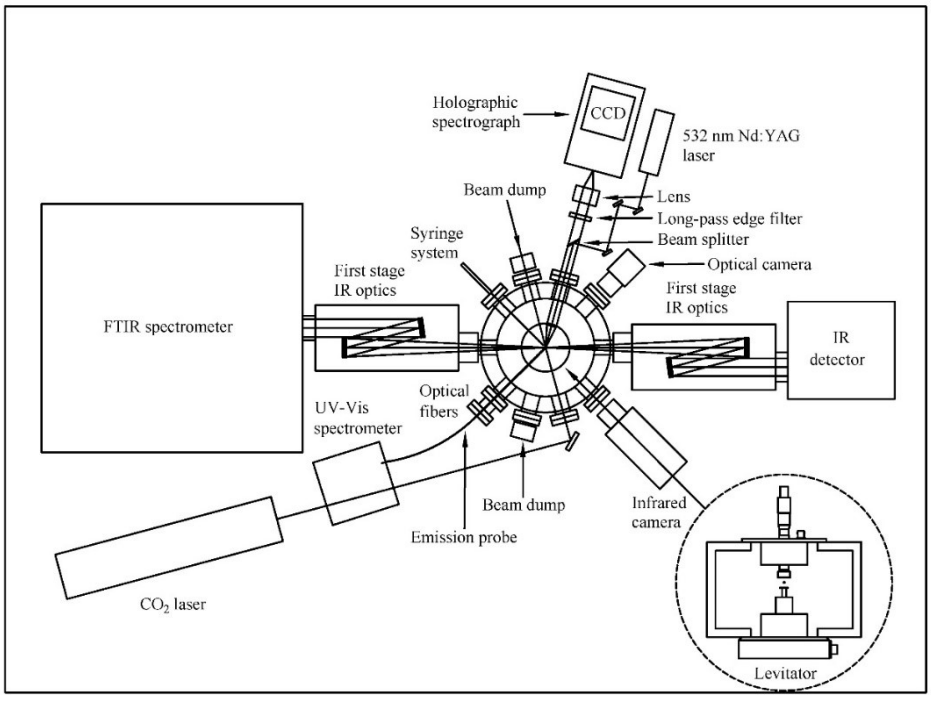

Figure S1. Schematic top view of the complete levitator apparatus displaying the ultrasonic levitator, process chamber, carbon dioxide laser, Raman, FTIR and fiber optic UV-vis spectrometer along with high-speed infrared and optical camera.[3]

S1.2. The process chamber and sampling system: The levitator assembly is enclosed within a pressure-compatible process chamber with a total volume of about 15 liters made of stainless steel to permit levitation in an inert gas or a highly reactive gas to investigate chemical reactions (Figure S2). The process chamber is also surrounded by spectroscopic (FTIR, Raman and UV-Vis spectrometers) as well as visualization tools (high-speed optical and infrared cameras) to identify any characteristic chemical or physical alterations of the levitated sample(s). In the present experiments, the chamber was filled with the mixture of argon and oxygen at the temperature and total pressure of 298 K and 900 Torr, respectively. To load chemically distinct droplets in adjacent pressure nodes of the levitator, two syringes are attached to an outside port on the chamber. Each syringe is connected via chemically inert teflon tubing to one of two microneedles inside the chamber. The pair of needles is attached to the end of a wobble stick. This dual droplet deposition system enables either needle tip to be precisely positioned within the second or third pressure minimum to load a droplet before being withdrawn to a rest position prior to the experiments.

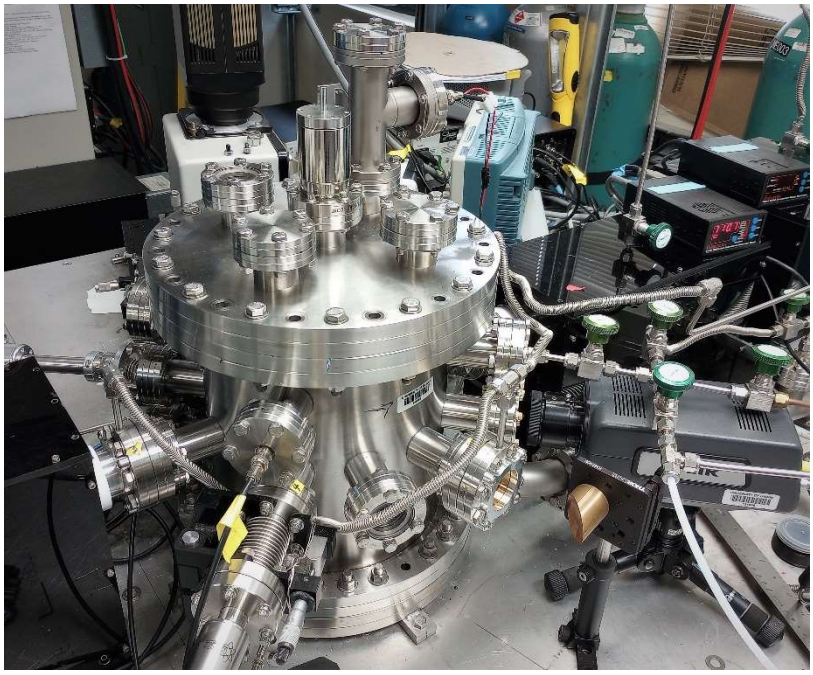

Figure S2. Side view of the levitator experimental setup containing the levitation device.

S1.3. Droplet merging: First, one droplet of the ionic liquid ([EMIM][CBH]) was loaded in the second pressure minimum above the ultrasonic transducer; hereafter the droplet of the oxidizer, white fuming HNO_3 (WFNA) was dispensed into the pressure minimum above. Second, the

chirped pulse of 1 s duration with the modulation voltage of typically 600-900 mV was applied to tune in for the resonant frequency. Initially the droplets undergo only non-axisymmetric oscillations, which were not sufficient to de-trap or dislocate them out of the acoustic potential wells. Third, as soon as the resonant frequency for the axial oscillations was attained in the chirp, there occurs a deformation in one of the droplets, making it a prolate spheroid from an oblate one along the vertical axis. The oscillation was further amplified due to the significantly high value of modulation voltage applied. Due to this excitation to the resonant normal mode of the droplet, it initiated a vertical oscillation and further merged with the other droplet positioned at the alternate pressure node driven by the surface tension. The merging motion can be initiated in either of the droplets, depending upon the size and mass.[2]

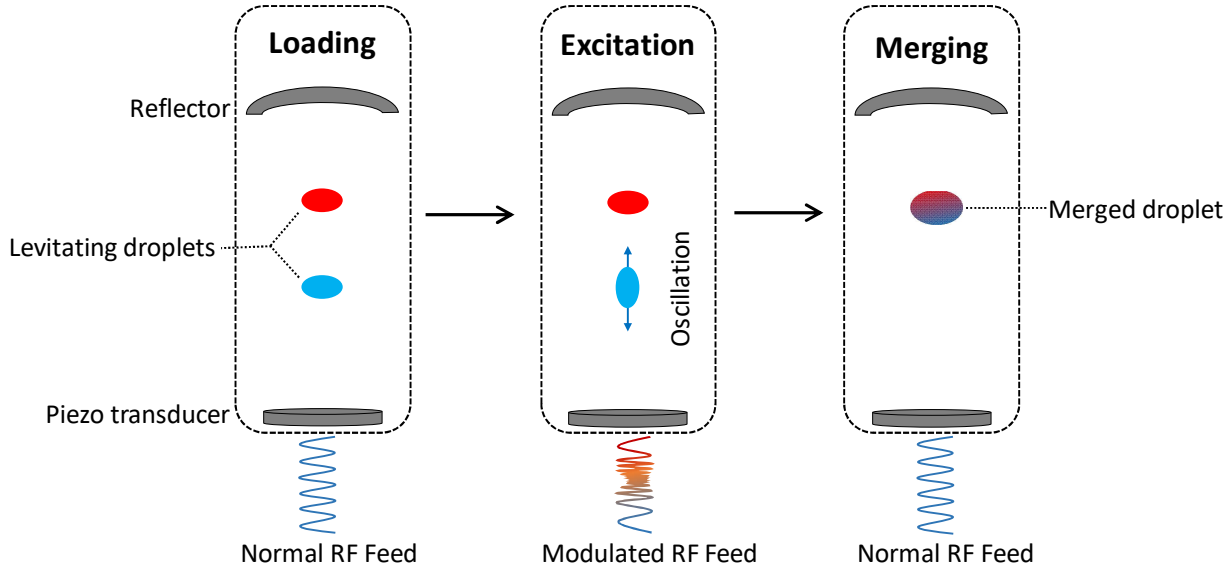

Figure S3. Schematic of droplet merging approach in the ultrasonic levitator utilizing an externally triggered chirped pulse in the range of 1-50 Hz to match the modulation frequency.

S1.4. UV-vis spectroscopy: In the UV-vis spectrometer system, the end of a fiber-optic probe is attached to an x, y, z manipulator located inside the process chamber. The manipulator enables the probe to be precisely aligned on the droplets at a distance of approximately 10-15 mm. The

electromagnetic radiation emitted by the flame upon ignition due to droplet merging is collected by the optical fiber, exits the chamber via a conflat fiber-optic feedthrough, and finally enters a StellarNet SILVER-Nova UV-vis spectrometer. The spectrometer operates in the 200-1100 nm spectral range with a resolution at full-width half-maximum (fwhm) of 2 nm and is capable of measuring emission spectral traces resulting from flame in a millisecond temporal resolution.

S1.5. FTIR spectroscopy. The gases produced by the merging of the droplets followed by ignition were identified by collecting an FTIR transmission spectrum in the 400-4000 cm^{-1} wavenumber region through the full width of the process chamber. The FTIR spectrometer system combines a Nicolet 6700 FTIR spectrometer (Thermo Scientific) with two stages of copper mirror optics. The infrared incident beam from the spectrometer was focused into a diameter of 4 mm around the levitated sample before re-collimating prior to detection by a liquid nitrogen cooled MCT-B (mercury cadmium telluride, wide band) detector. The acquisition time for each spectrum was 15 s at a spectral resolution of is 4 cm^{-1} for the instrument. In the experiment, to get the FTIR spectrum for the newly generated gaseous products, first a background spectrum was recorded immediately after loading the droplets; which was then subtracted from the spectrum acquired after ignition event. The number densities or number of moles of the gases (for hydrogen cyanide (HCN), nitrous oxide (N_2O), nitrogen dioxide (NO_2), and nitric oxide (NO)) evolved during merging events followed by ignition were evaluated from the previously recorded calibration curves obtained by taking different pressures of the respective gases individually in the process chamber maintaining the identical experimental conditions.[2] Similarly, carbon dioxide (CO_2) was also quantified by using a new calibration curve (Figure S4). To find out the number of moles for nitrous acid (HONO), the infrared absorption cross section value at 1264 cm^{-1} was used.[4]

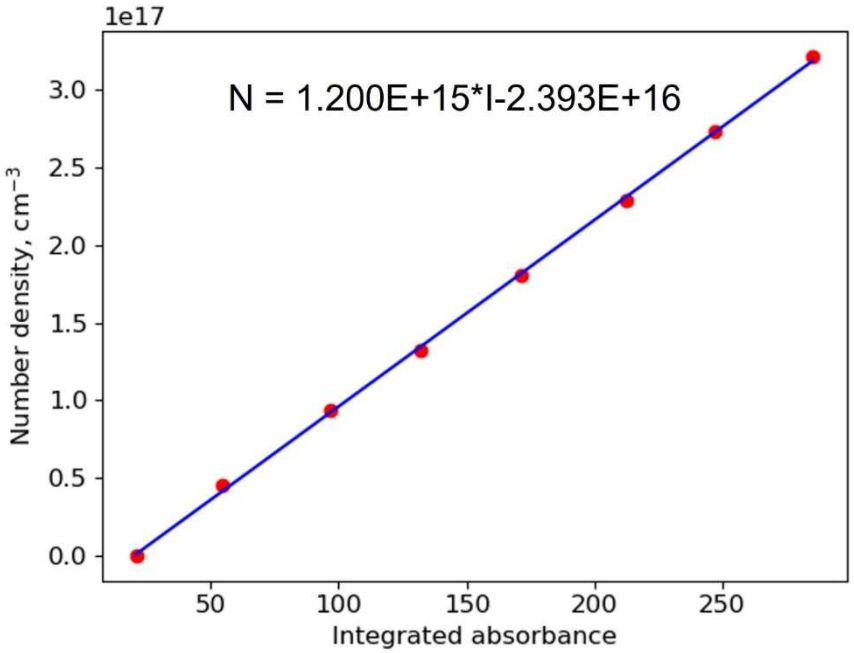

Figure S4. Calibration of FTIR signal for carbon dioxide (CO_2). Integrated area for the CO_2 antisymmetric stretch band in the 2170-2460 cm^{-1} range was used.

S1.6. The optical and infrared movies and snapshots: To record high-speed events, a Phantom Miro 3a10 camera operating at repetition rate up to 1 kHz combined with a Navitar Zoom 6000 modular lens system was aligned on the levitated sample via an optical viewport. Infrared thermal imaging videos of the merging events were recorded using an FLIR A6703sc camera. The camera was set to a repetition rate of 250 Hz and the infrared camera was also partially used to determine temperature changes of the levitated droplets while merging. Both of the optical and IR camera were triggered externally by the pulse generator synchronized with the UV-Vis spectrometer.

S1.7. Pulse sequence: The droplet merging and the successive ignition event occur at a few milliseconds time regime; therefore, each spectroscopic as well as visual detection methods needed to be synchronized. For this purpose, all of the data collection tools except the FTIR spectrometer were synchronized and externally triggered by a pulse generator, (Quantum Composer Plus, model-9518) operating at 1 kHz repetition rate. A schematic of the typical pulse sequencing is depicted in Figure S5.

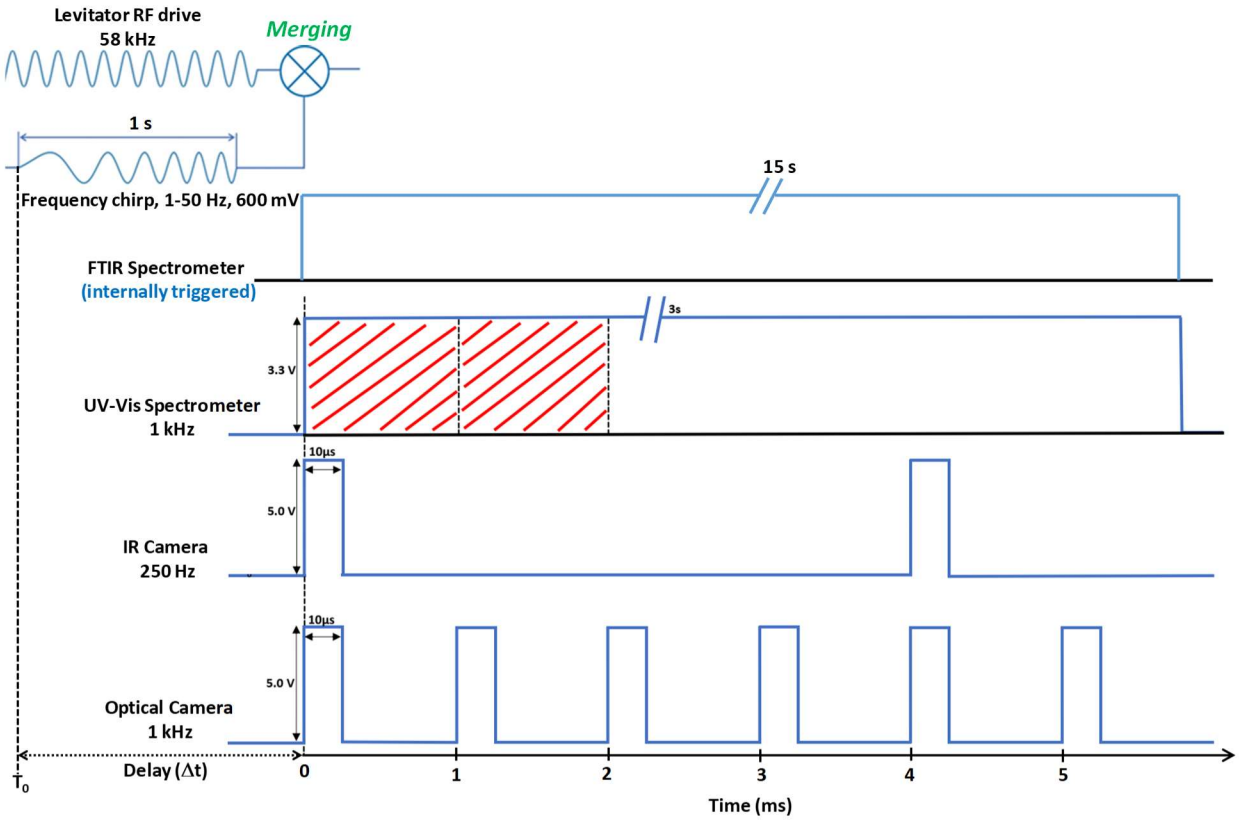

Figure S5. Typical pulse sequence used for operation of the ultrasonic levitator, droplet merging and data recording.

The merging-up chirp, which was generated by the waveform/function generator was triggered in a single-shot mode, spanning 1 s. The UV-Vis spectrometer to detect the intermediate species formed during the ignition was also triggered in single-shot mode with a typical delay of 100 ms since trigger (T_0), enabled to capture 127 consecutive spectral traces with a temporal resolution of 2 ms. On the other hand, the optical and infrared camera were operated in burst mode which implies the number of pulses were limited to a certain value. As the infrared camera was only capable of operating up to one-fourth of the trigger repetition rate, it was synchronized by providing 3 milliseconds wait time with respect to T_0, which captured thermal images every fourth pulse from T_0, thus, it was synchronized with the optical video frames.

S1.8. Chemicals and gases used: The sample 1-ethyl-3-methylimidazolium cyanoborohydride was synthesized in house[5] and white fuming nitric acid (HNO_3,100%) was procured from Sigma Aldrich. Argon (99.9999%, Ar) and molecular oxygen (100%, O_2) gas to fill the levitator process

chamber were procured from Airgas. The gases for the calibration purposes were supplied by Matheson Tri-gas: carbon dioxide (CO_2, purity: 99.999%) hydrogen cyanide (HCN, diluted 5% in helium), nitrous oxide (N_2O, purity: 99.999%), nitric oxide (NO, diluted 1% in argon), nitrogen dioxide (NO_2, diluted 0.5% in argon).

S2. Computational method

In a recent computational study[6], the primary decomposition pathway of the CBH^- + HNO_3 reaction was investigated at the B3LYP/6-31G* level of theory.[7, 8] In the hope of identifying non-intuitive reaction pathways, the critical points are searched in an unsupervised manner and ~3,000 of them were found. One often overlooked aspect in characterizing the potential energy profile is how thorough the search is for optimal structures. Traditionally, the optimal structures have largely been identified following chemical intuition by making guesses of the structures of the intermediates (e.g., *via* addition or insertion of separated reactants) and proposed possible isomerizations that eventually lead to products reported by experiment. This method has seen great successes in *validating* reaction mechanisms by confirming the hypothesized mechanisms with quantum chemistry calculations, e.g., the excess energy in the system allows for certain reactions to take place. However, when it comes to *exploring* a new reaction pathway that is out of the realm of chemical intuition, this method bares its shortcomings. Once the most obvious, intuitive pathways are confirmed, further searching is prematurely stopped. Take the most fundamental S_N2 reaction, $F^- + CH_3I \rightarrow CH_3F + I^-$, as an example, whose potential energy profile is believed to be the traditional Walden inversion pathway with C_{3v} symmetry until around 2008. Guided-beam experiments and AIMD simulations then revealed counterintuitive scattering angle distribution at low collision energy instead of the traditionally believed forward scattering, which inspired chemists to conduct a more thorough search and revealed many other reaction pathways.[9]

To mitigate the limitations of chemical intuition, the optimal structures are searched thoroughly in an unsupervised fashion. Two molecular representations are adopted to identify, sort through, and categorize these structures. The first one is a distance matrix (DM) - an *N* by *N* symmetric matrix, where *N* is the number of atoms, whose elements are:

$$DM_{i,j} = \begin{cases} 0 & if\ i = j \\ 1/r_{i,j} & if\ i \neq j \end{cases}$$

i and j are the indexes of a pair of atoms and $r_{i,j}$ is the distance between them. DM is invariant to rotation and translation, thus is an ideal molecular representation in dealing with a large number of molecular configurations. The distance matrix deviation (DMD) between two configurations is defined as the norm of the difference between their corresponding DMs, minimized over all possible permutations of indistinguishable atoms. DMD is used to determine whether two configurations are identical. DMs can be further processed to edge-adjacency matrices (EMs), whose elements are:

$$EM_{i,j} = \begin{cases} 0 & if\ r_{i,j} > r_{cut} \\ 1 & if\ r_{i,j} \leq r_{cut} \end{cases}$$

i, j, and $r_{i,j}$ take the previous definition while r_{cut} = 2.20 Å is an empirical distance set to detect whether there exists (i.e., $EM_{i,j}$ = 1) a chemical bond between a pair of atoms, with the exception of hydrogen which is restricted to having at most one bond. The edge-adjacency matrix deviation (EMD) is defined in the same way as DMD to determine whether two configurations have the same connectivity. In this way, molecules of the same distinct molecular graph (EMD = 0) may be grouped first and different conformers (DMD > 0.001 A^{-1}) will be distinguished among them.

One way of constructing molecular graphs of distinct EMs is made from the association of separated species. These species could be separated reactants or products (identified by the experiments), which are randomly oriented and set apart by different distances. The system is allowed to evolve following the energy gradient, mostly likely leading to the association between these species and formation of intermediates. The molecular graphs corresponding to those intermediates are good candidates for initial geometry for optimization, as they potentially represent the first (in the case of reactants) or the last (in the case of products) step of the chemical reaction. Another way of constructing molecular graphs of distinct EMs is AIMD simulations. The EMs of each frame of the AIMD trajectories are calculated and tallied, and those highly populated EMs are used as initial geometries to optimize. These geometries are ideal candidates for intermediates as their high population in the trajectories implies a low free energy. These two arguments carry little to no chemical intuition in generating initial geometries and have been reported to identify counterintuitive reaction pathways of low barrier.[6]

In the present case, the determined critical points lead to a total of eight gas phase primary products with low (e.g., ~ 30 kJ mol^{-1}) overall barriers. Experiments under similar excess energy (e.g., at room temperature) identified four of those.[2] The remaining molecules accompanying the formation of these experimentally identified products are further studied for O_2 addition at the same level of theory. The N-boryl-N-oxo-formamide (BOFA) doublet radical anion ($HCON(O)BH_3^-$) was chosen for its low O_2 additional barrier. It is important to note that there are *five* potential sites of O_2 addition and different levels of theory have reported different intermediates, but only those that can be (1) confirmed with CCSD(T)/cc-pVDZ[10, 11] geometry optimization and (2) are within 30 kJ mol^{-1} of the separated reactants are reported as the focus is to find the initial ignition step of the reaction. Only the Van der Waals (vdW) complex is valid for O_2 addition in the current system and its further decomposition pathways are explored with B3LYP/6-31G*, as it has been shown to characterize the reaction pathways that agree with the experiment. The electronic energy is refined with CCSD(T)/cc-pVDZ, which is then corrected by relative free energy at 298.15 K. Intermediates and separated reactant/products are confirmed to have 3N-6 (3N-5 for linear molecules) positive vibrational frequencies while transition states are confirmed to have 3N-7 (3N-6 for linear molecules) positive vibrational frequency with a single imaginary frequency. The connection between the transition states and their corresponding intermediates are confirmed with intrinsic reaction coordinate (IRC) calculations with the Gonzalez-Schlegel algorithm.[12, 13] Intermediates are classified as Van der Waals (vdW) complexes when two or more distinct molecular fragments exist (> ~180 pm apart). It is also important to point out that for a floppy system, the reported intermediates are distinguished only by connectivity, which could include multiple conformers differing by e.g., the rotation of a sigma bond and the *cis*/*trans* interconversion. In such cases, the conformer of the lowest energy is reported on the potential energy surface. All calculations were carried out with NWChem version 6.8.[14]

Table S1. Droplet sizes of the reactants and percentage of molecular oxygen (O_2) used in different experimental sets. The errors originate from the measurement errors of the major and minor axes of the levitating oblate spheroid droplets.

Droplet index	Percentage of molecular O_2	Volume of [EMIM][CBH] (μl)	Mean volume (μl)	Volume of WFNA (μl)	Mean volume (μl)
1	0%	5.6 ± 3.0	5.5 ± 2.8	8.1 ± 4.0	8.1 ± 4.0
2	0%	4.9 ± 2.0		8.3 ± 4.0	
3	0%	5.1 ± 3.0		8.4 ± 4.0	
4	0%	6.3 ± 3.0		7.6 ± 4.0	
1	10%	10.2 ± 5.0	7.8 ± 4.0	10.9 ± 5.0	10.8 ± 5.2
2	10%	8.7 ± 4.0		12.0 ± 6.0	
3	10%	5.2 ± 3.0		10.2 ± 5.0	
4	10%	7.3 ± 4.0		10.2 ± 5.0	
1	20%	9.1 ± 5.0	9.8 ± 5.0	8.6 ± 4.0	9.6 ± 4.8
2	20%	10.7 ± 5.0		9.2 ± 5.0	
3	20%	9.2 ± 5.0		7.8 ± 4.0	
4	20%	10.2 ± 5.0		13.0 ± 6.0	
1	30%	11.8 ± 6.0	13.0 ± 6.5	12.5 ± 6.0	10.7 ± 5.2
2	30%	16.4 ± 8.0		14.3 ± 7.0	
3	30%	12.1 ± 6.0		7.3 ± 4.0	
4	30%	11.7 ± 6.0		8.7 ± 4.0	
1	40%	10.3 ± 1.0	10.9 ± 4.5	8.0 ± 8.0	10.6 ± 6.5
2	40%	10.4 ± 5.0		11.2 ± 6.0	
3	40%	15.2 ± 8.0		14.1 ± 7.0	
4	40%	7.8 ± 4.0		9.3 ± 5.0	
1	50%	7.0 ± 7.0	8.8 ± 6.0	2.7 ± 3.0	6.9 ± 5.5
2	50%	8.1 ± 5.0		8.4 ± 6.0	
3	50%	9.7 ± 7.0		7.4 ± 6.0	
4	50%	10.2 ± 5.0		8.9 ± 7.0	
1	60%	11.6 ± 2.0	8.3 ± 2.8	7.3 ± 7.0	8.1 ± 5.5
2	60%	7.6 ± 3.0		8.7 ± 4.0	
3	60%	6.2 ± 3.0		7.5 ± 5.0	
4	60%	7.9 ± 4.0		9.1 ± 6.0	

Table S2. Number of moles of the reactants with the varying molecular oxygen (O_2) contents in the levitator process chamber along with measured ignition delays (ID). The errors in the number of moles originate from the measurement errors of the volume of the levitating oblate spheroid droplets while the errors in the ignition delays represent the 1-σ errors in the averaged time differentials between individual merging and ignition frames.

Percentage of molecular O_2	Number of moles for molecular O_2	Number of moles for [EMIM][CBH] ($\times 10^{-5}$)	Number of moles for WFNA ($\times 10^{-4}$)	Molar ratio [EMIM][CBH]:WFNA	Ignition delay (ms)
0 %	0	3.6 ± 1.8	1.9 ± 1.0	1: 5.3 ± 1.2	No ignition
10 %	0.07 ± 0.01	5.1 ± 2.6	2.6 ± 1.2	1: 5.1 ± 3.1	15 ± 7
20 %	0.14 ± 0.01	6.4 ± 3.2	2.3 ± 1.1	1: 3.6 ± 1.7	12 ± 5
30 %	0.21 ± 0.01	8.4 ± 4.2	2.6 ± 1.2	1: 3.1 ± 1.5	8 ± 3
40 %	0.28 ± 0.02	7.1 ± 2.9	2.5 ± 1.6	1: 3.5 ± 1.8	4 ± 1
50 %	0.35 ± 0.02	5.7 ± 3.9	1.7 ± 1.3	1: 3.0 ± 1.7	4 ± 2
60 %	0.42 ± 0.02	5.4 ± 1.8	1.9 ± 1.3	1: 3.5 ± 1.9	3 ± 2

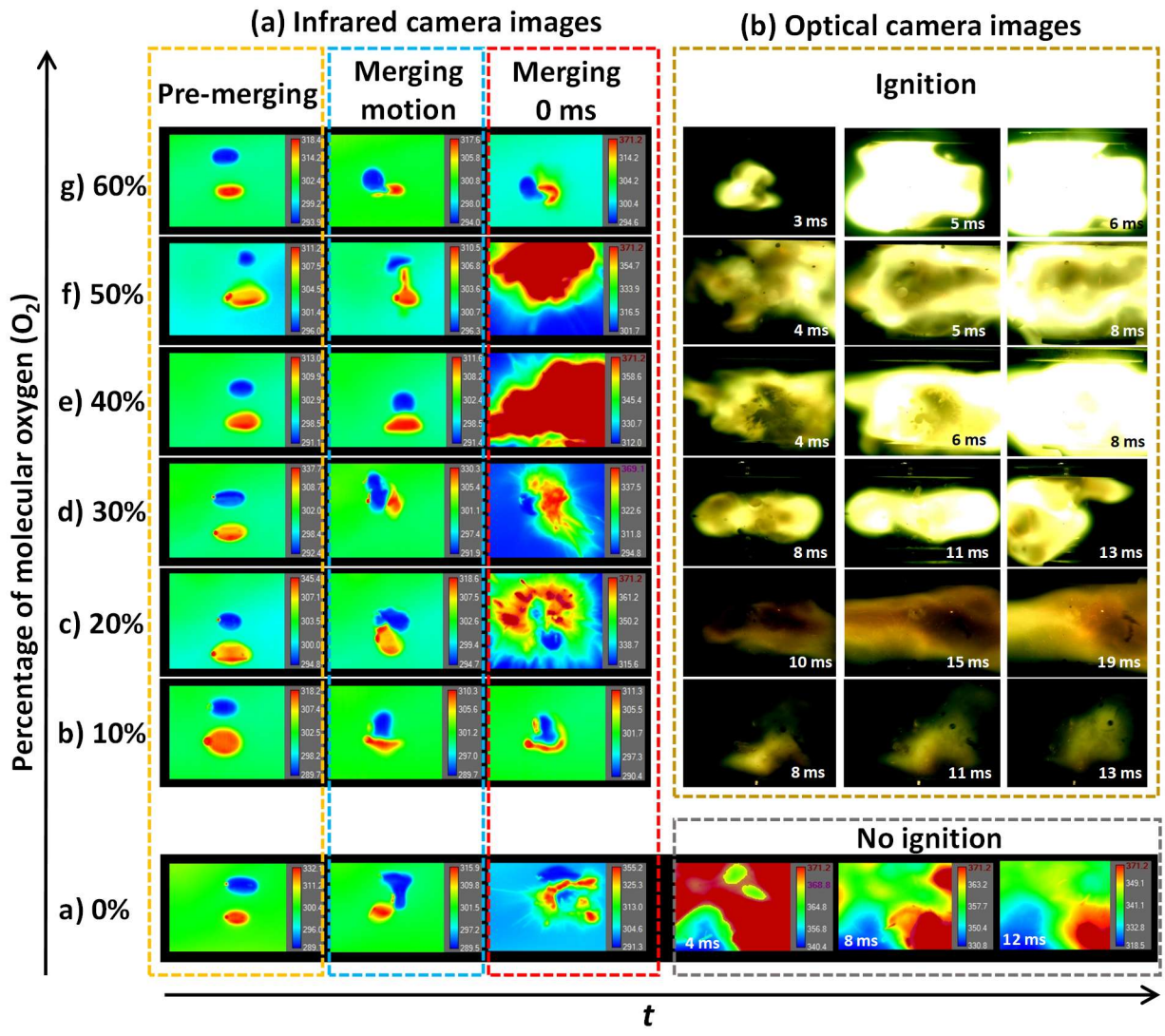

Figure S6. High-speed images captured by the synchronized (a) infrared camera and (b) optical camera to depict merging sequence between the levitating droplets of [EMIM][CBH] (bottom) and WFNA (top) followed by ignition at different fractions of molecular O_2-contents. The infrared camera captures the merging instance, while the optical camera indicates the commencement of ignition.

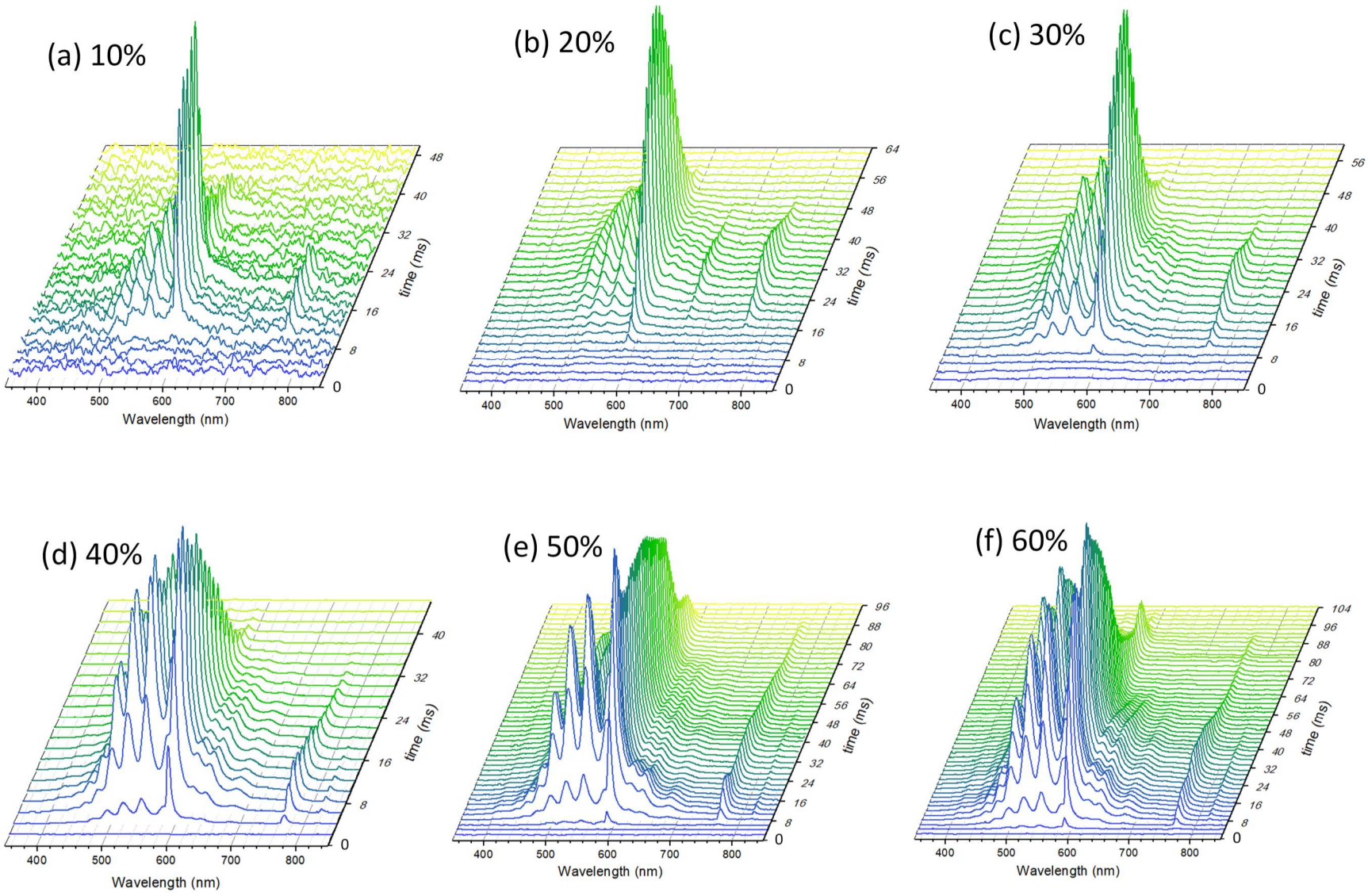

Figure S7. Temporal evolution of the flame emission spectra for the ignition occurred due to merging between [EMIM][CBH] and WFNA droplets upon varying molecular O_2-contents.

Table S3. Peak/band assignments for the deconvoluted flame emission spectra of [EMIM][CBH] - WFNA ignition reaction.

Peak /band	Peak wavelength / band center (nm)	Species	Reference wavelength (nm)	Transition	Branch; spin-orbit components; vibrational quantum numbers: (ν', ν'') or (ν_1',ν_2',ν_3') - (ν_1'',ν_2'',ν_3'')
a	408.9 ± 1.9	BO_2	407.5[a]	$B\ ^2\Sigma^+_u - X\ ^2\Pi_g$	(0,0); (1,1); (2,2)
b	434.5 ± 1.2	BO_2/ CH	431.2[a]/ 431.4[b]	$A\ ^2\Pi_u - X\ ^2\Pi_g$/ $A\ ^2\Delta - X\ ^2\Pi$	(0,2,n)-(0,0,n); (0,3,n)-(1,1,n)/ (0,0)
c	453.1 ± 0.6	BO_2	448.8[a]	$A\ ^2\Pi_u - X\ ^2\Pi_g$	(n,2,m)-(n-2,2,m); (n,3,0)-(n-1,3,m)
d	473.7 ± 1.1	BO_2	469.6[a]	$A\ ^2\Pi_u - X\ ^2\Pi_g$	(n,2,m)-(n-1,2,m); (n,1,m)-(n-2,1,m)
e	495.4 ± 0.8	BO_2	492.7[a]	$A\ ^2\Pi_u - X\ ^2\Pi_g$	(n,0,m)-(n-2,0,m); (n,1,m)-(n-1,1,m)
f	520.2 ± 0.5	BO_2	518.1[a]	$A\ ^2\Pi_u - X\ ^2\Pi_g$	(n,0,m)-(n-1,0,m), (n,1,m)-(n,1,m)
g	548.4 ± 1.4	BO_2	546.5[a]	$A\ ^2\Pi_u - X\ ^2\Pi_g$	(n,0,m)-(n,0,m)
h	581.2 ± 0.7	BO_2	581.2[a]	$A\ ^2\Pi_u - X\ ^2\Pi_g$	(n,0,m)-(n+1,0,m)
i	589.1 ± 1.4	Na	589.0[c]	$2p^63p\ ^2P^o - 2p^63s\ ^2S$	3/2 - 1/2
j	590.5 ± 1.3	Na	589.6[c]	$2p^63p\ ^2P^o - 2p^63s\ ^2S$	1/2 -1/2
k	623.1 ± 1.7	BO_2	620.2[a]	$A\ ^2\Pi_u - X\ ^2\Pi_g$	(n,0,m)-(n+2,0,m)
l	641.1 ± 1.8	BO_2	644.2[a]	$A\ ^2\Pi_u - X\ ^2\Pi_g$	(n,0,m)-(n+3,0,m)
m	681.8 ± 1.1	BO_2	687.8[a]	$A\ ^2\Pi_u - X\ ^2\Pi_g$	(0,0,m)-(1,2,m)
n	768.5 ± 0.3	K	766.5[c]	$3p^64p\ ^2P^o - 3p^64s\ ^2S$	3/2 - 1/2
o	772.6 ± 0.4	K	769.9[c]	$3p^64p\ ^2P^o - 3p^64s\ ^2S$	1/2 - 1/2
p	819.9 ± 0.4	Na	818.3, 819.5[c]	$2p^63d\ ^2D - 2p^63p\ ^2P^o$	5/2 - 3/2; 3/2 - 3/2; 3/2 - 1/2

a - reference 15, 16; b - reference 17; c – reference 18.

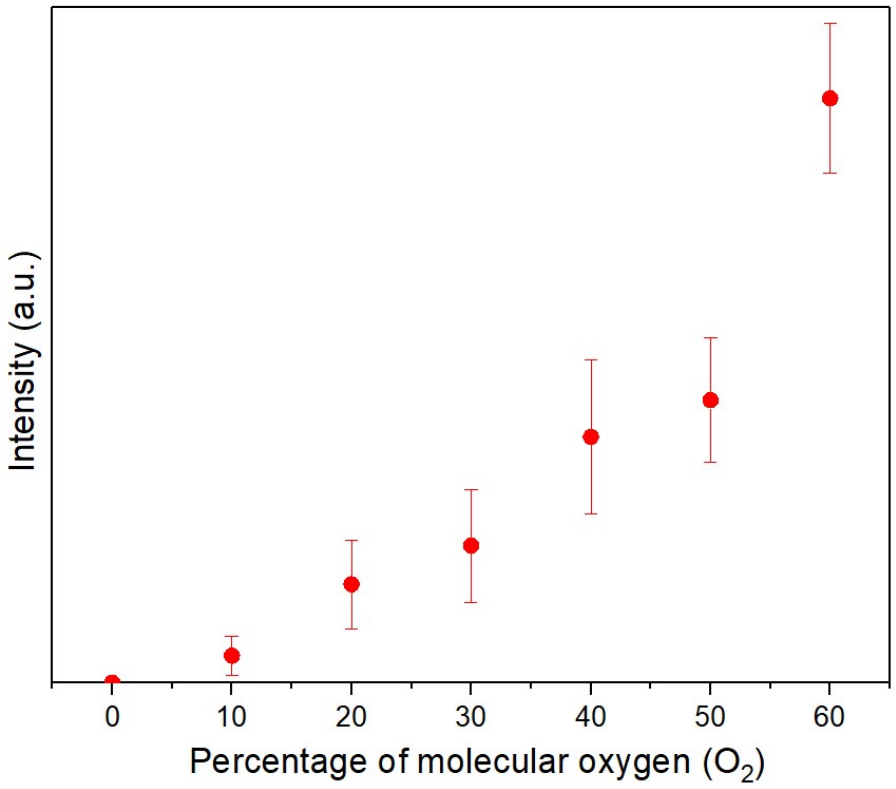

Figure S8. Maximum emission intensities as a function of molecular oxygen (O_2) contents for the [EMIM][CBH] – WFNA ignition reaction. The errors in the intensities represent the 1-σ errors in the averaged emission profiles.

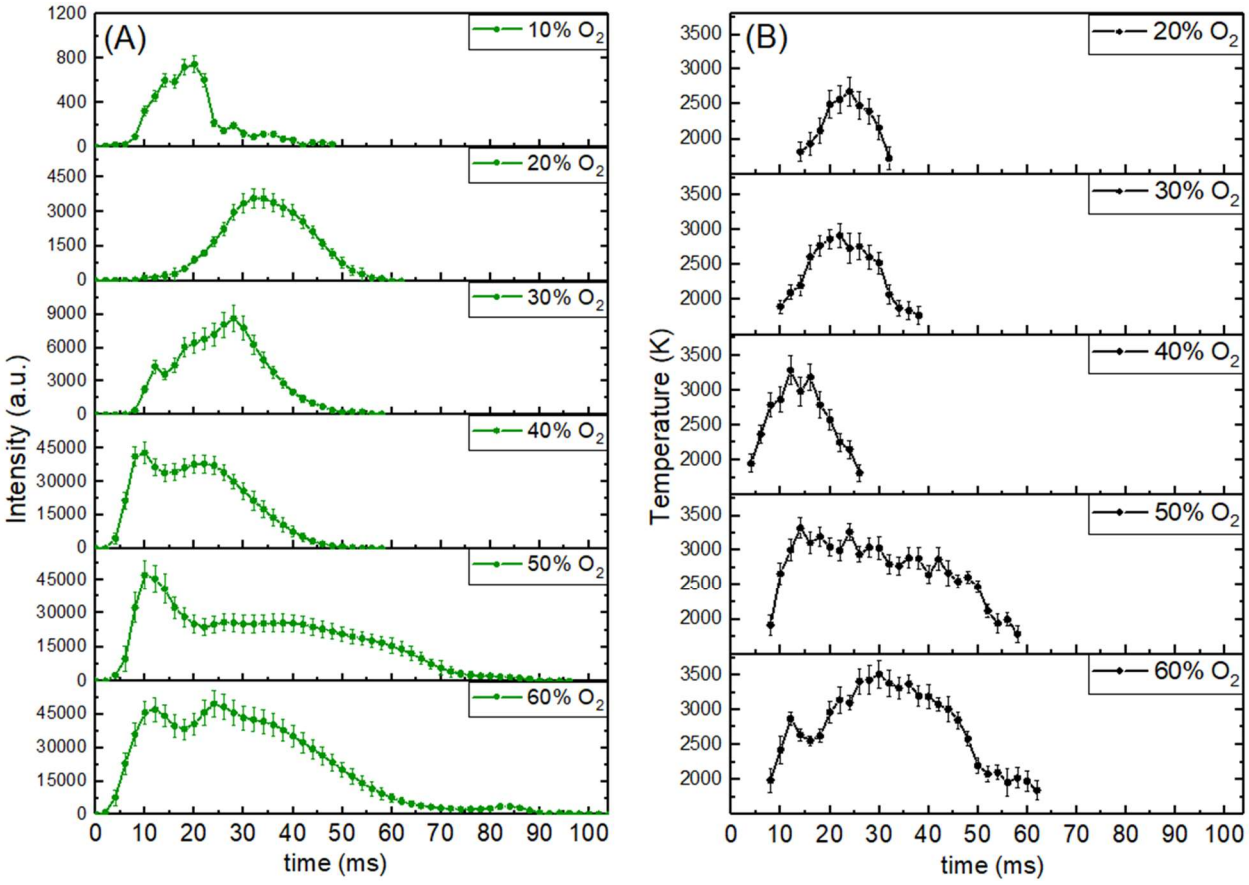

Figure S9. Temporal profiles of (A) boron dioxide (BO_2) and (B) flame temperature in the [EMIM][CBH]-WFNA ignition reaction at different molecular O_2 volume fractions.

Table S4. Number of moles of the gaseous products formed after merging at different molecular oxygen (O_2) concentrations inside the process chamber. The errors in the number of moles consist of the uncertainties in the FTIR measurements and calibration curves.

Percentage of molecular O_2	HCN ($\times 10^{-6}$)	N_2O ($\times 10^{-6}$)	NO_2 ($\times 10^{-6}$)	CO_2 ($\times 10^{-5}$)	HONO ($\times 10^{-6}$)	NO ($\times 10^{-6}$)
0 %	12.8 ± 2.4	29.3 ± 2.0	16.1 ± 0.8	0	0	0
10 %	6.2 ± 1.5	12.7 ± 1.5	0.8 ± 0.1	13.6 ± 1.2	0.002 ± 0.001	0
20 %	1.3 ± 0.5	14.3 ± 1.9	3.0 ± 0.4	14.2 ± 1.8	0.004 ± 0.0011	0
30 %	2.3 ± 0.6	8.7 ± 1.2	6.2 ± 0.7	16.5 ± 1.7	0.006 ± 0.0014	0
40 %	2.5 ± 0.4	2.9 ± 0.3	7.0 ± 0.5	19.7 ± 1.8	0.008 ± 0.0017	0
50 %	0.4 ± 0.2	3.7 ± 0.2	7.8 ± 0.8	25.1 ± 2.2	0.019 ± 0.0022	0.06 ± 0.017
60 %	0.4 ± 0.1	0.8 ± 0.2	5.8 ± 0.5	29.9 ± 3.2	0.017 ± 0.0024	0.13 ± 0.02

Table S5. Percentage yield of carbon dioxide (CO_2) from the $[EMIM]^+$ cation during combustion. The errors in the number of moles for molecular O_2 originate from the 1-σ errors in the averaged partial pressures of O_2 in the process chamber, while the errors in the number of moles of the $[EMIM]^+$ originate from the volume measurement errors of the droplets. The errors in number of moles of CO_2 is consisted of the uncertainties in the FTIR measurements and calibration curves.

Percentage of molecular O_2	Number of moles for molecular O_2	Number of moles for $[EMIM]^+$ ($\times 10^{-5}$)	Number of moles of CO_2 ($\times 10^{-5}$)	Percentage yield from $[EMIM]^+$
0 %	0	3.6 ± 1.8	0	0
10 %	0.07 ± 0.01	5.1 ± 2.6	13.6 ± 1.2	45 %
20 %	0.14 ± 0.01	6.4 ± 3.2	14.2 ± 1.8	37 %
30 %	0.21 ± 0.01	8.4 ± 4.2	16.5 ± 1.7	33 %
40 %	0.28 ± 0.02	7.1 ± 2.9	19.7 ± 1.8	46 %
50 %	0.35 ± 0.02	5.7 ± 3.9	25.1 ± 2.2	73 %
60 %	0.42 ± 0.02	5.4 ± 1.8	29.9 ± 3.2	87 %

S3. Deconvolution of flame emission spectra upon ignition

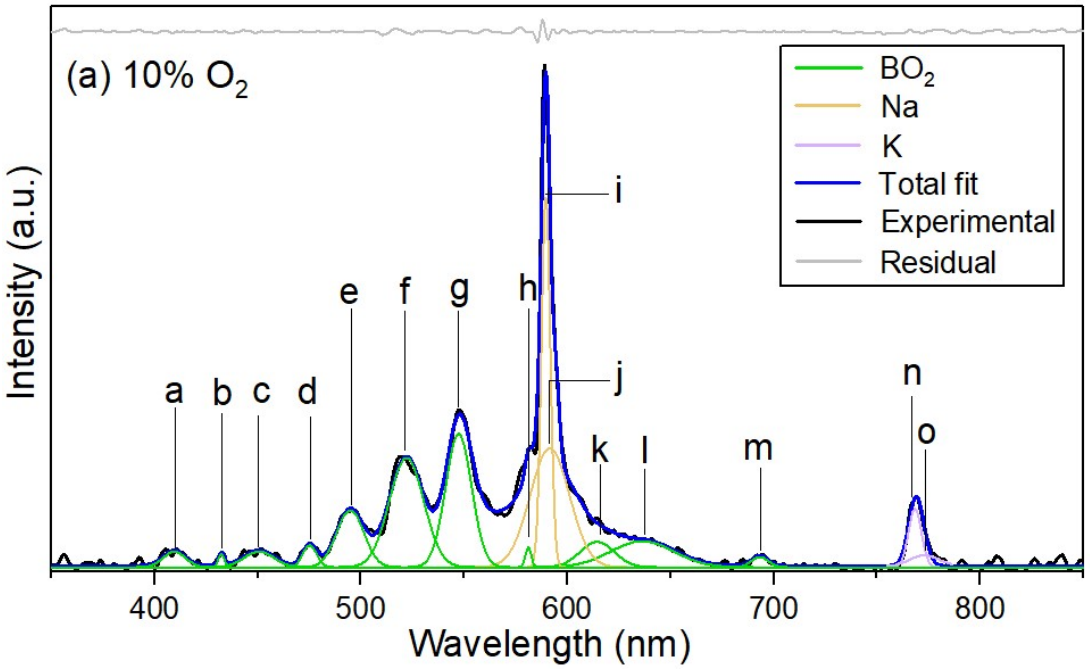

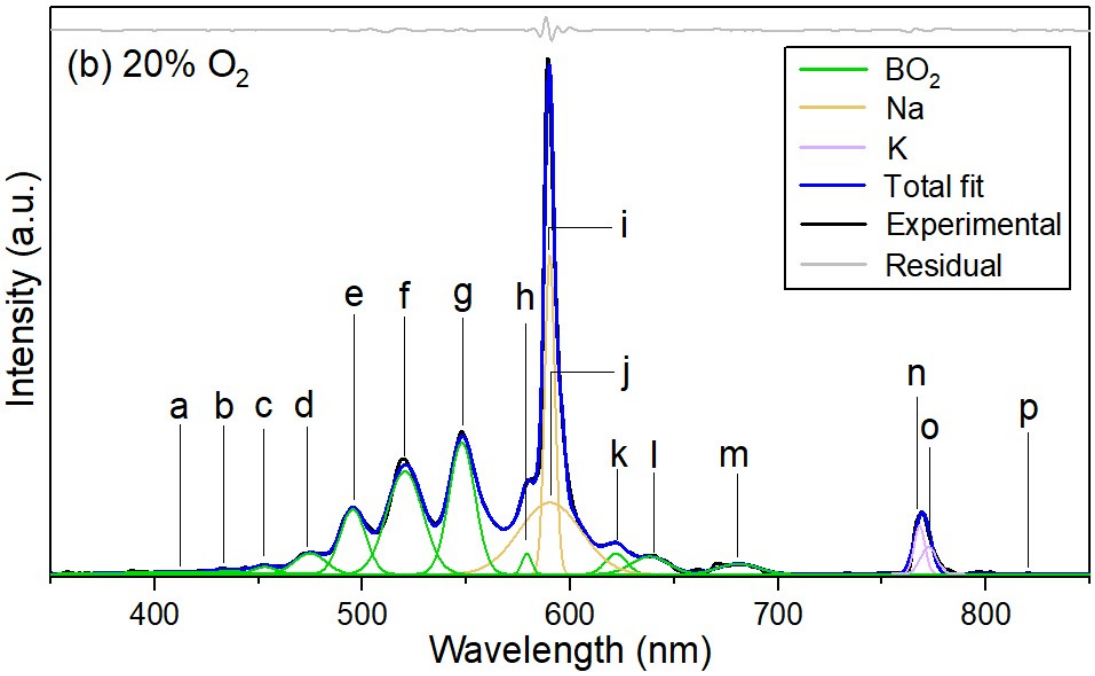

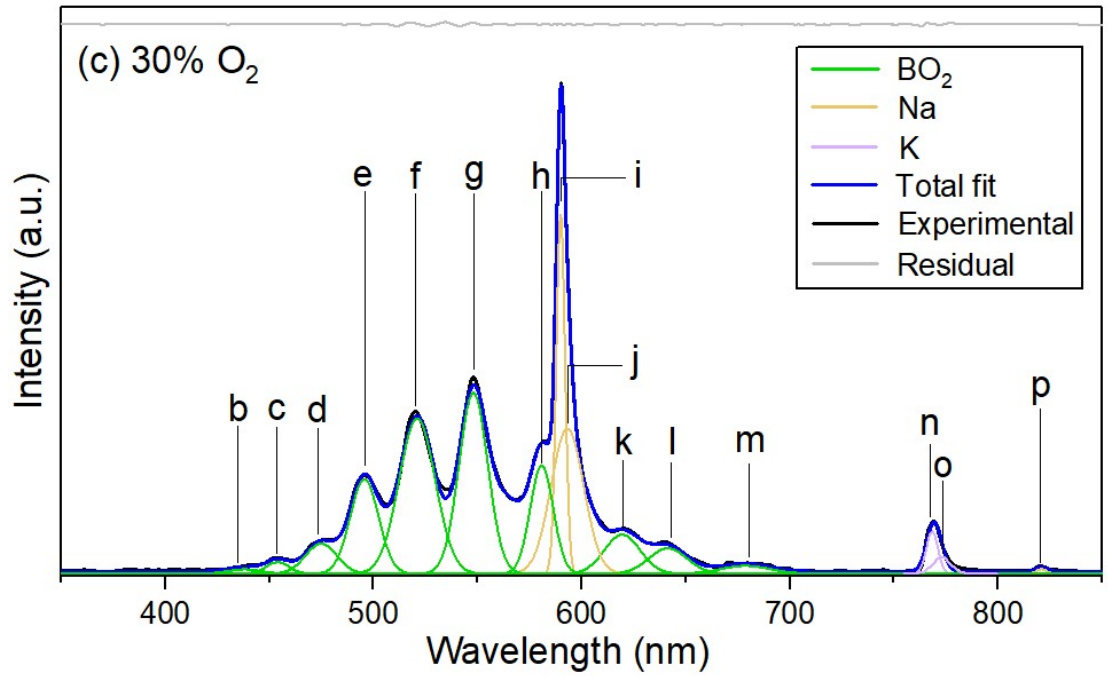
(c) 30% O_2
BO_2
Na
K
Total fit
Experimental
Residual
Intensity (a.u.)
b c d e f g h i j k l m n o p
400 500 600 700 800
Wavelength (nm)

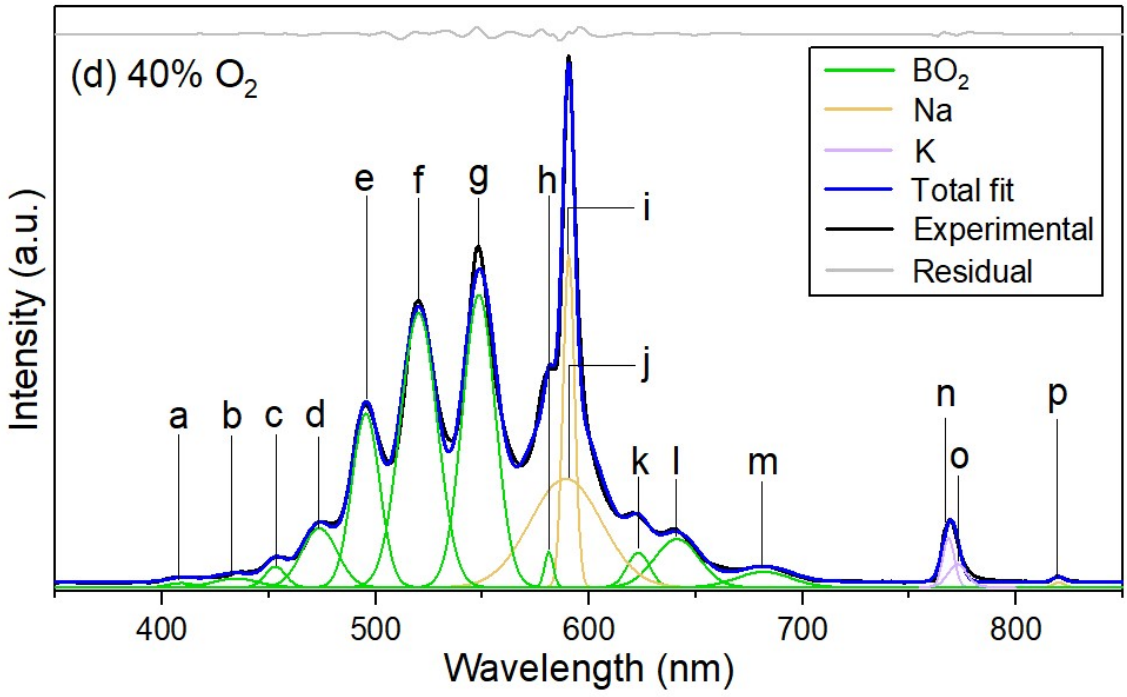
(d) 40% O_2
BO_2
Na
K
Total fit
Experimental
Residual
Intensity (a.u.)
a b c d e f g h i j k l m n o p
400 500 600 700 800
Wavelength (nm)

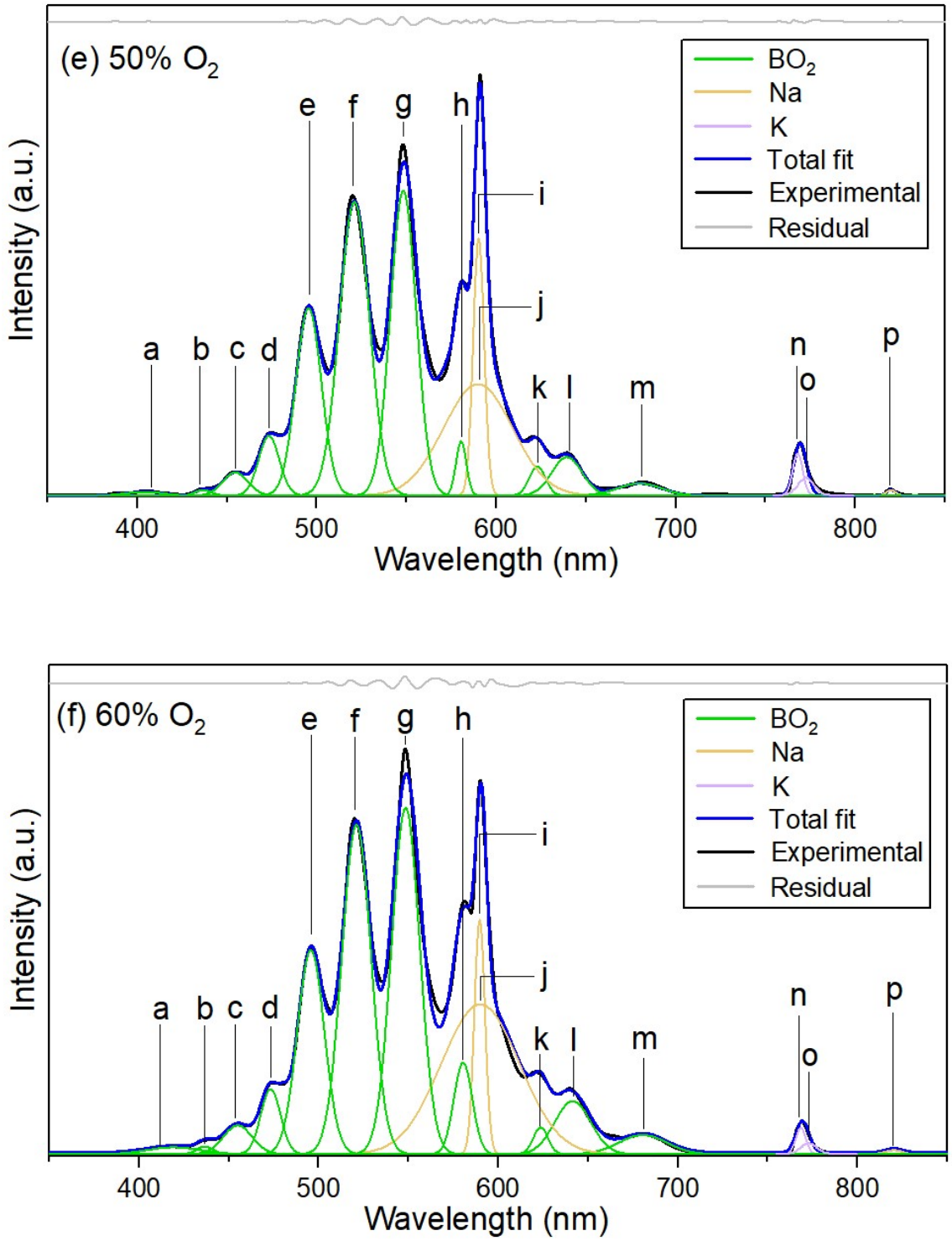

Figure S10. Deconvolution of the flame emission spectra for the ignition reaction of [EMIM][CBH] ionic liquid with white fuming nitric acid (WFNA) as a function of molecular oxygen (O_2) contents of- (a) 10%, (b) 20%, (c) 30%, (d) 40%, (e) 50% and (f) 60%.[18]

S4. Temporal profiles of the intermediates during ignition

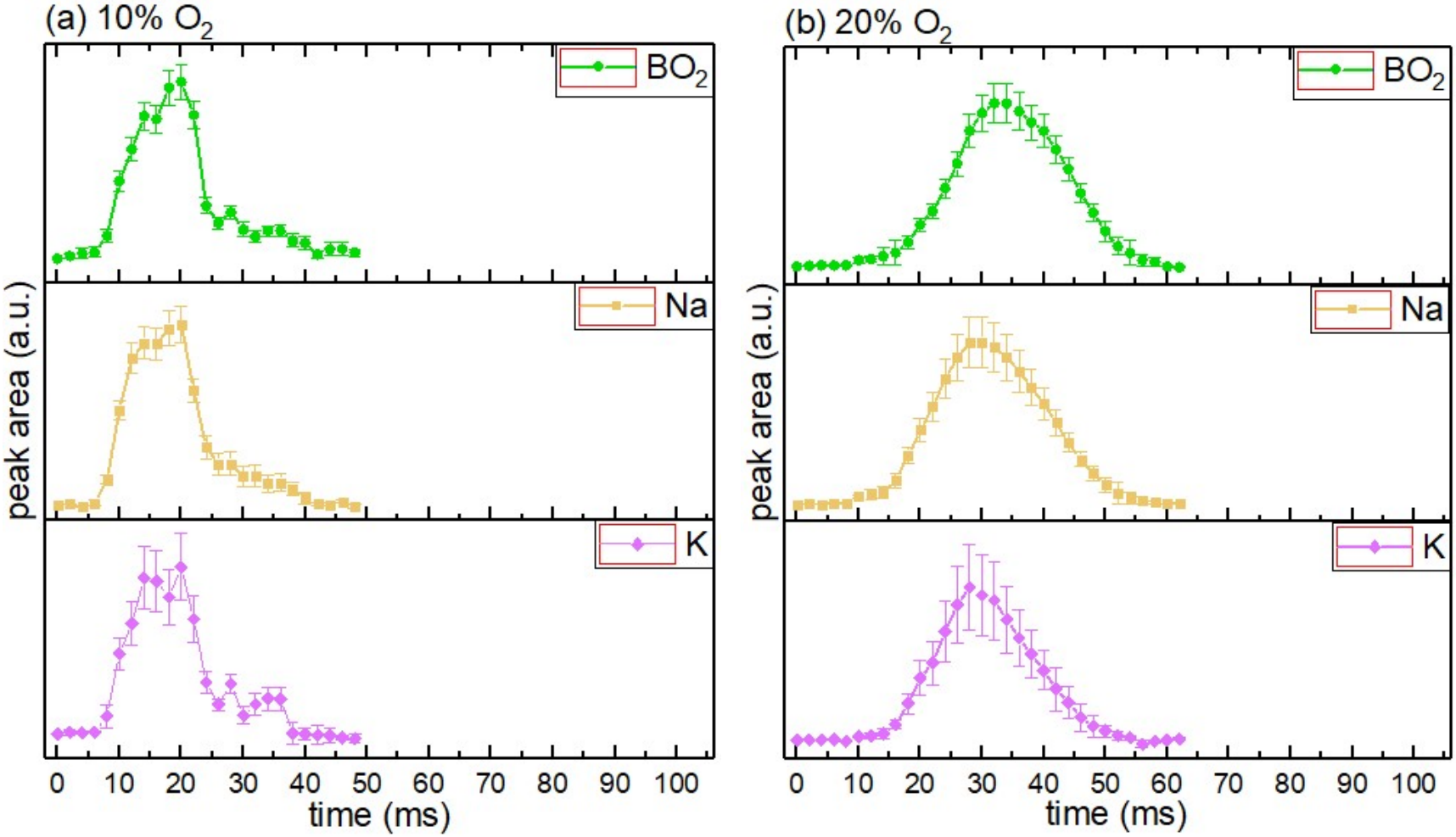

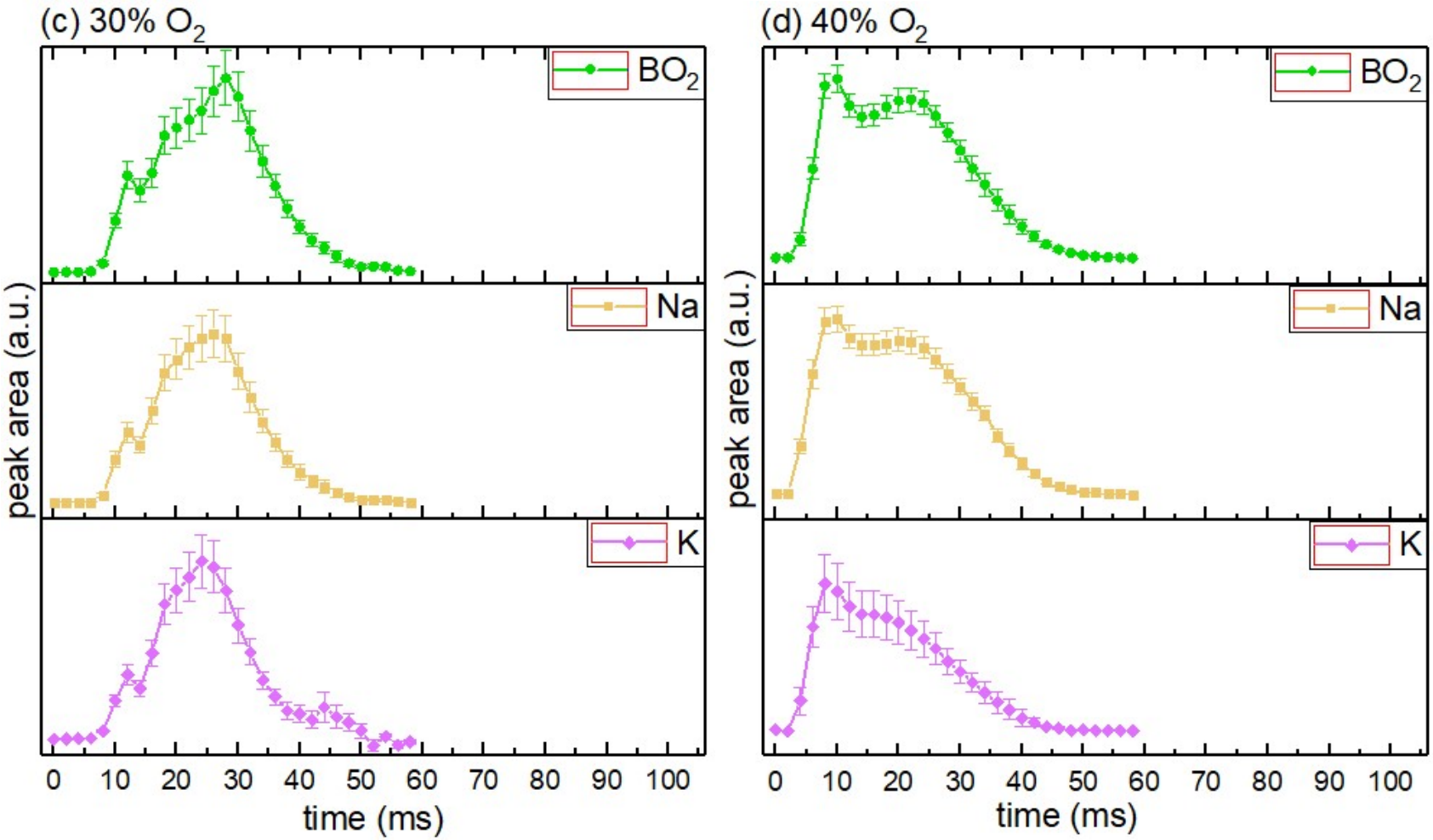
(c) 30% O2
(d) 40% O2
BO2
Na
K
peak area (a.u.)
time (ms)
0
10
20
30
40
50
60
70
80
90
100

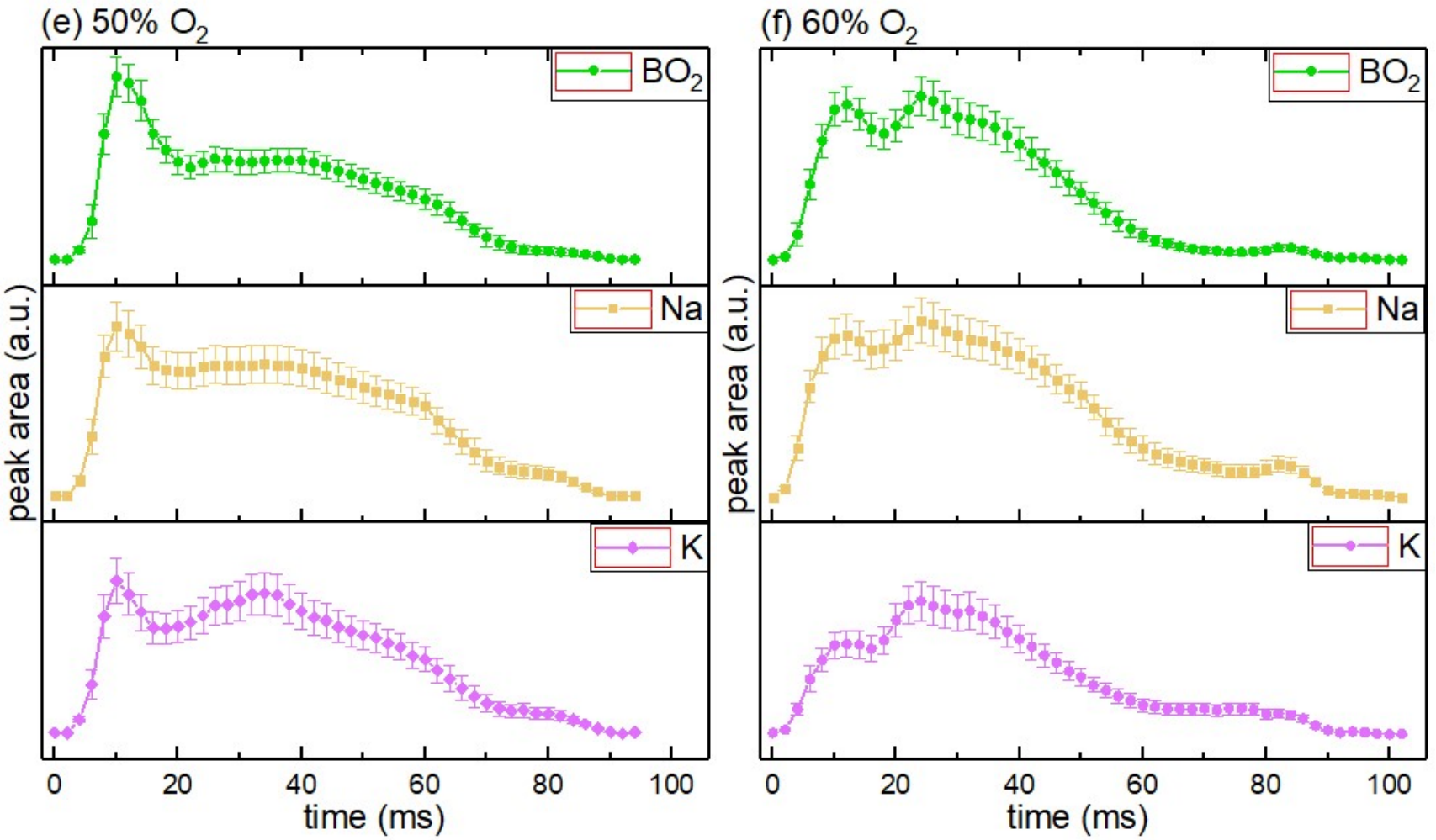

Figure S11. Temporal profiles of boron dioxide (BO_2), sodium (Na), and potassium (K) atoms in the reaction of [EMIM][CBH] ionic liquid with WFNA as a function of molecular O_2 contents of- (a) 10%, (b) 20%, (c) 30%, (d) 40%, (e) 50% and (f) 60%. The extraction of the temporal plots was performed by using the source code published earlier.[19]

S5. Flame temperature

The relative intensities of the two atomic emission lines (say from *m* and *n* state) incorporating the Boltzmann population distribution can be expressed as-

$$\frac{I_n}{I_m} = \frac{A_n g_n \upsilon_n}{A_m g_m \upsilon_m} exp[-(E_n - E_m)/kT] \quad \text{(Eq. S1)}$$

Where, for *m* and *n*-states: A_m, A_n are the emission transition probabilities of the radiation (s^{-1}); g_m, g_n are the statistical weights of the respective levels [= (2J +1), J represents the total electronic angular momentum]; ($A_m g_m$), ($A_n g_n$) are the weighted transition probabilities (s^{-1}); ν_m, ν_n are the emission frequencies (cm^{-1}); E_m, E_n are the absolute energies (cm^{-1}); respectively and k is Boltzmann constant. If the abovementioned parameters are known,[18] then utilizing the relative intensity ratio of the two atomic emission lines, temperature of the flame, T can be determined.

In this work, two emission lines of sodium (Na) have been considered to estimate the flame temperature, which are located at 589 (3p→3s) and 819.5 nm (3d→3p). The required parameters have been adopted from the NIST Atomic Spectra Database.[18] The weighted transition probabilities used for 589 and 819.5 nm bands are 2.46×10^8 and 3.08×10^8 s^{-1}, respectively.

S6. Coordinates for the optimized structures including transition states (TS) in the potential energy surface (PES)

BOFA				**i1**			
B	0.08150596	-1.19316805	-1.49551177	O	-2.46231317	-0.62240761	-0.92702451
C	0.78242528	0.52881918	0.33714490	O	-2.07564616	-0.13210045	0.12584881
H	1.25795797	-1.05193320	-1.81054578	B	0.81820262	0.20029782	-1.72106857
H	1.74086167	0.41589263	-0.20040354	C	0.61615968	0.87822589	0.79437954
H	-0.66131291	-0.83636083	-2.40061903	H	0.00387278	-0.59203150	-2.17812448
H	-0.15060462	-2.35082356	-1.17257466	H	0.22183698	1.79131181	0.31769894
N	-0.20123603	-0.27151585	-0.24135042	H	1.91827923	0.02333149	-2.22343444
O	-1.36845951	-0.22608957	0.29958349	H	0.43654210	1.35382346	-1.86339658
O	0.64692832	1.26941302	1.30697300	N	0.95027337	-0.08292254	-0.17582558
				O	1.41396356	-1.19105001	0.26348303

				O	0.75347996	0.75662719	2.00411093
i2				**i3**			
O	-2.18928728	-0.61220324	-0.84563591	O	-1.59263140	0.73771588	1.45730173
O	-2.79052043	0.56478635	-0.64874007	O	-2.00345745	-0.25143405	0.66161533
B	0.82879855	0.20118041	-1.56229210	B	-0.86952189	-1.20158770	0.17888536
C	0.65654032	0.70157354	0.79963221	C	0.81086828	-0.18904308	-1.50985451
H	-1.20821187	-0.41217903	-0.81399670	H	0.25012793	0.69190532	1.24555147
H	-0.12051110	1.38365136	0.40621239	H	0.20612767	-0.78978654	-2.22246972
H	1.31506781	-0.39690651	-2.47720794	H	-0.59710643	-1.92654513	1.11894647
H	0.01190503	1.06471280	-1.73181804	H	-1.35171352	-1.78929257	-0.76940340
N	1.24854740	-0.08188840	-0.23135447	N	0.33660548	-0.38191416	-0.26490041
O	2.16632608	-0.94457151	0.12004458	O	1.02416542	0.31301599	0.76699611
O	0.95373922	0.64616079	1.97827595	O	1.76743394	0.49395082	-1.87735879
i4				**i5**			
O	-2.34085906	0.70951920	0.18849494	O	-1.13259901	-1.73955744	0.38379241
O	-1.46928639	0.97542244	-0.97647685	O	-1.28054703	0.34739534	1.60555733
B	-0.11135195	1.21469751	-0.51783977	B	-1.19418783	-0.28885253	0.30878263
C	1.84497950	-0.53749901	-0.18513529	C	0.87835921	-0.33394874	-1.39397183
H	0.00765619	2.02032155	0.39762926	H	-0.66505184	1.09998941	1.54991754
H	2.34780749	0.20435224	-0.83113534	H	0.32787396	-1.24083458	-1.69601827
H	-1.85055899	-0.05647646	0.55995583	H	-0.66957609	-1.91777998	1.21765280
H	0.54656576	1.52349715	-1.50274333	H	-2.03951279	0.03415497	-0.52997728
N	0.52075786	-0.17036658	0.03421607	N	0.24277319	0.27729608	-0.32218161
O	-0.19595202	-0.97295356	0.75111493	O	0.77016009	1.35347963	0.15852959
O	2.41173229	-1.52958400	0.25649335	O	1.90846204	0.03948210	-1.94841815
i6				**i7**			
O	-1.00431926	-0.61192655	1.83562860	B	-0.81019175	-0.97624909	-0.08836791
O	-1.74138003	1.14645400	0.23041656	C	0.76359077	1.02611940	-0.08097978
B	-1.06293569	-0.09101229	0.55111886	H	-0.15338025	1.62789779	-0.14065761
C	0.76343120	0.50188221	-1.26048409	H	-2.67555039	1.51796547	0.93201677
H	-2.48182806	1.18949120	0.85179829	H	-2.18473229	0.68235217	-0.23440828

H	-0.01319847	1.21411756	-1.60502928	H	2.39740562	-0.31966943	0.03987416
H	0.66127945	-1.26022721	1.22617110	N	0.52658075	-0.30074055	-0.05133174
H	-1.73981690	-1.14992501	0.14806915	O	-2.67374215	1.53932605	-0.03875138
N	0.31398291	-0.13265881	-0.17119859	O	1.74796396	-1.06321766	0.03435324
O	1.17374114	-1.10547402	0.39585089	O	1.90863294	1.51283444	-0.03926159
O	1.84993142	0.37641022	-1.83757397	O	-1.14842807	-2.18857909	-0.03954196
i8				**i9**			
O	-0.92989087	0.22424002	1.47317186	B	1.34511613	0.16949497	-0.00299442
O	-3.20688606	0.23743408	2.09037844	C	-1.05699225	0.99126979	-0.15617001
B	-2.19126379	-0.13397546	1.21533865	H	-0.88190576	1.92338945	0.40285856
C	1.91109129	0.11544063	-2.06426243	H	-1.89566096	-0.59543548	0.08285688
H	-2.78406579	0.74997309	2.79893290	N	-0.01680093	0.01627510	-0.02871126
H	1.96453391	0.96982363	-2.78060371	O	-0.50652971	-1.30072230	-0.02288340
H	-0.22479349	-0.07845749	0.77005316	O	-2.25712802	0.38256377	0.07758362
H	-2.55027269	-0.77899924	0.26478834	O	2.57057861	0.33256780	0.02942614
N	0.96332840	0.40797762	-1.09794326				
O	0.82817510	-0.55616765	-0.21212623				
O	2.63462752	-0.87492785	-2.21057160				
i10				**i11**			
B	1.04276198	0.01744614	0.13065181	B	0.97085304	-0.07247787	0.03442590
C	-1.31562557	-0.24614029	-0.15297789	C	-1.61963968	0.51223415	0.03441927
H	-1.21516064	-1.12544613	-0.80162457	H	-2.23587121	1.45117863	0.03448621
H	-2.64198119	0.81712645	0.60060161	H	-0.09023958	1.78041861	0.03474636
N	-0.40693653	0.42479697	0.38650272	N	-0.29689077	0.78630673	0.03466180
O	1.97771347	0.94051351	-0.11539256	O	2.14052666	0.55753579	0.03412996
O	-2.66323427	0.03929891	0.01047295	O	-2.17681453	-0.57962706	0.03416244
O	1.43579530	-1.25867177	0.12637595	O	0.96900001	-1.40824674	0.03455469
p1				**p2**			
B	1.38984377	-0.65744420	-0.00349568	C	-0.05834299	-0.50935720	-0.74564177
C	-1.13635980	-0.78660693	-0.00356163	H	-0.75392619	0.72653036	1.95569118
H	-0.95049207	-1.87078322	-0.00350352	H	-0.51018873	-1.33179535	-1.32527507

H	-1.27578667	1.33625138	-0.00367557	N	-0.76893583	-0.33481515	0.45064594
N	0.00075794	-0.07010407	-0.00342712	O	-0.20394244	0.67631164	1.15250280
O	-0.29080153	1.37656649	-0.00357065	O	0.90965848	0.12786302	-1.11926353
O	-2.28133430	-0.29433131	-0.00373097	**p2_H_2BO_2**			
O	2.53613295	-0.12871661	-0.00374039	O	-0.66840960	0.93670979	0.26393707
p1_H_2O				H	-0.43089660	0.71915694	1.18231881
O	0.00000000	0.06700105	0.05293575	B	-0.08902178	-0.19289432	-0.44329931
H	0.76156262	-0.53172115	0.05293575	O	0.54629527	-1.15855094	0.12495350
H	-0.76156262	-0.53172115	0.05293575	H	-0.32207469	-0.04293778	-1.65711230
p3				**p4**			
C	-0.07086063	-0.63653741	-0.48705846	C	0.46210472	0.02334181	0.12370956
H	-0.62673068	-1.55856649	-0.80566998	H	1.39960783	-0.56371010	-0.07565143
N	-0.74484256	-0.06888917	0.57815864	H	-1.32372026	-0.25422184	-0.49361675
O	-0.18306408	1.02216014	1.03763960	N	0.22174549	1.02416034	0.78222001
O	0.96539012	-0.30273291	-1.08609180	O	-0.52790147	-0.78647692	-0.68706923
p3_H_3BO_2				**p4_BO_2**			
O	0.02461069	-1.17530776	-0.43220739	O	1.26574164	0.03876793	-0.06532813
O	0.32652415	0.86057857	0.71498686	O	-1.26338364	0.03876793	-0.06532813
B	-0.13148727	0.17370432	-0.37751365	B	0.00118141	0.03884284	-0.06532813
H	0.16032133	1.80974149	0.64172736				
H	0.47143654	-1.50655885	0.36359573				
H	-0.67031820	0.71449048	-1.29893816				
p5							
C	-0.00192997	-0.30380871	0.03898759				
H	0.01611835	-1.45147393	0.03899113				
H	1.87987562	-0.45836524	0.03898867				
N	1.17903946	0.29689509	0.03898853				
O	-1.14335876	0.21936860	0.03898855				
p5_BO_2							
O	1.26574164	0.03876793	-0.06532813				
O	-1.26338364	0.03876793	-0.06532813				

B	0.00118141	0.03884284	-0.06532813				
Transition States							
i1_i2				**i2_i3**			
O	-2.03624645	-0.47188829	-1.13979078	O	-1.51049931	1.30871010	1.07915603
O	-2.15309947	-0.12919824	0.09810701	O	-2.74260637	0.89826001	1.39982005
B	0.62647126	0.14071765	-1.57755170	B	-0.38101581	-1.70318795	0.26119717
C	0.57830320	0.83183025	0.80418552	C	0.71810840	-0.08389387	-1.15847229
H	-0.76414626	-0.27980190	-1.43974354	H	-0.98974843	0.47638104	0.90503494
H	0.02924862	1.66993507	0.34689912	H	-0.19642222	-0.27312450	-1.75261548
H	1.12052075	-0.58321111	-2.40146003	H	-0.40874740	-2.38794261	1.24145347
H	0.39151238	1.29861862	-1.83736098	H	-1.23802344	-1.75902356	-0.57609922
N	1.01395932	-0.11105234	-0.18448718	N	0.70929541	-0.80463406	0.06916971
O	1.64607874	-1.13823177	0.24969483	O	1.73731393	-0.64455596	0.87101888
O	0.82981354	0.75349026	1.98885037	O	1.61234923	0.64766919	-1.53871463
i3_i4				**i4_i5**			
O	-1.93177613	0.54742838	0.68176823	O	-1.13040674	-0.84641773	1.44617601
O	-1.58241074	1.28847486	-0.45612217	O	-1.73393202	1.00094296	1.81019879
B	-0.14189164	1.17075566	-0.79499848	B	-0.76751245	-0.80699140	0.12510151
C	1.65883927	-0.42835503	0.15492606	C	0.93957616	-0.16877800	-1.61561848
H	0.53501091	2.05229280	-0.27171979	H	-0.78332817	1.20930067	1.86568683
H	2.28895536	0.46906564	-0.01255546	H	0.20249823	-0.70183939	-2.24392771
H	-1.36355287	-0.47344121	0.38532205	H	-0.55899715	-1.93376212	0.89659550
H	-0.09502849	1.27465880	-2.01616510	H	-1.50524365	-1.01675326	-0.81375393
N	0.39601292	-0.19278281	-0.29854385	N	0.52188132	-0.12643147	-0.28210420
O	-0.53031949	-1.17222301	-0.14377941	O	1.28163256	0.48090434	0.57439038
O	2.10948919	-1.46735176	0.63223585	O	1.97031120	0.30586325	-2.06469592
i5_i6				**i6_i7**			
O	-0.97682483	-0.77854952	1.69363440	B	-1.08601064	-0.21318009	-0.35942020
O	-1.88211025	1.10530584	0.37376669	C	1.29856750	0.74732409	-0.26983899
B	-1.19115097	-0.16797508	0.47654355	H	0.83966095	1.68880991	-0.59658266
C	0.77960798	0.38692566	-1.37173748	H	-2.45411032	1.43665313	0.35341001

H	-1.78773846	1.49856684	1.25383549	H	-1.33453528	0.77273147	-1.12984656
H	-0.00723259	1.01869082	-1.82859468	H	1.94439493	-1.14611862	0.39215083
H	0.38858926	-1.10129453	1.28086395	N	0.41230174	-0.24381428	-0.11449021
H	-1.69285346	-0.97767314	-0.36009532	O	-1.53726742	1.76707550	0.31629969
N	0.32372349	-0.09834390	-0.19820523	O	1.00433732	-1.44428863	0.33533842
O	1.11688668	-0.95600948	0.50839477	O	2.51990048	0.61111977	-0.04926639
O	1.89303351	0.23857059	-1.88558190	O	-1.94655551	-1.12243949	-0.12626150
i5_i8				**p1_i9**			
O	-1.06549737	-1.03881716	1.59146237	B	1.40154468	-0.14181720	0.00714730
O	-2.02657144	1.06663941	0.89372244	C	-1.02397836	-1.00115121	-0.10671820
B	-1.75587373	-0.28211148	0.67018101	H	-0.85763847	-1.90536881	0.50422886
C	1.06238931	0.32603799	-1.60241498	H	-1.69644927	0.68292453	0.04214647
H	-1.43204925	1.34921096	1.60709467	N	0.04026731	-0.01492210	0.00523628
H	0.28747012	0.66115971	-2.32673846	O	-0.51757658	1.28381046	0.00003565
H	-0.08251776	-0.93201789	1.41209627	O	-2.19153082	-0.35591025	0.04799937
H	-2.45254882	-0.78046859	-0.18136428	O	2.62871413	-0.29622967	0.01819006
N	0.44125549	-0.09370073	-0.44062263				
O	1.24893054	-0.49660655	0.50200550				
O	2.26213973	0.35367482	-1.88944087				
i9_i10				**i10_i11**			
B	1.27872950	0.12058641	0.06760734	B	1.05118459	0.05165079	0.04383124
C	-1.18740868	0.87644665	0.08135798	C	-1.42467805	-0.41746595	0.03667788
H	-1.48870528	1.66431225	0.78997041	H	-1.38302347	-1.50810898	0.02354604
H	-1.65907235	-0.84163860	-0.30388407	H	-1.65508563	1.12188208	0.05441220
N	-0.04259453	0.12009898	0.48485417	N	-0.43464249	0.40668624	0.04685139
O	-0.15007913	-1.29338417	0.12354252	O	1.98958602	1.00148823	0.03898367
O	-2.20312759	0.02293356	-0.26189347	O	-2.57437703	0.21681329	0.04335487
O	2.47970818	0.24573103	-0.19744636	O	1.45995724	-1.21770932	0.04474386

Table S6. Enthalpy changes of the reactant droplets- ionic liquid ([EMIM][CBH]) and oxidizer (WFNA) during merging, considering the overall specific heat capacity to be 1.0 ± 0.2 $Jg^{-1}K^{-1}$. The resultant specific heat capacity of the liquid mixture was evaluated using the specific heat capacity values for similar type of ionic liquids containing $[EMIM]^+$ (2.0 $Jg^{-1}K^{-1}$) and WFNA (0.85 $Jg^{-1}K^{-1}$). The errors in the number of moles and masses originate from the measurement errors of the volume of the levitating oblate spheroid droplets.

Percentage of molecular O_2	Mass of [EMIM][CBH] droplet (kg) ($\times 10^{-6}$)	Number of moles for [EMIM][CBH] ($\times 10^{-5}$)	Mass of WFNA droplet (kg) ($\times 10^{-5}$)	Number of moles for WFNA ($\times 10^{-4}$)	Molar enthalpy change (kJ mol^{-1})
0 %	5.4 ± 2.7	3.6 ± 1.8	1.2 ± 0.6	1.9 ± 1.0	3.3 ± 1.2
10 %	7.7 ± 3.9	5.1 ± 2.6	1.6 ± 0.7	2.6 ± 1.2	6.1 ± 1.0
20 %	9.6 ± 4.9	6.4 ± 3.2	1.5 ± 0.7	2.3 ± 1.1	8.3 ± 0.9
30 %	12.6 ± 6.3	8.4 ± 4.2	1.6 ± 0.7	2.6 ± 1.2	8.7 ± 1.3
40 %	10.7 ± 4.4	7.1 ± 2.9	1.6 ± 0.9	2.5 ± 1.6	10.4 ± 1.1
50 %	8.6 ± 5.8	5.7 ± 3.9	1.1 ± 0.8	1.7 ± 1.3	10.1 ± 1.3
60 %	8.2 ± 2.7	5.4 ± 1.8	1.2 ± 0.8	1.9 ± 1.3	12.2 ± 1.3

Supplementary References:

1. S. J. Brotton and R. I. Kaiser, *Rev. Sci. Instrum.*, 2013, **84**, 055114.
2. S. Biswas, I. Antonov, K. Fujioka, G. L. Rizzo, S. D. Chambreau, S. Schneider, R. Sun and R. I. Kaiser, *Phys. Chem. Chem. Phys.*, 2023, **25**, 6602-6625.
3. S. J. Brotton and R. I. Kaiser, *Anal. Chem.*, 2020, **92**, 8371-8377.
4. W. S. Barney, L. M. Wingen, M. J. Lakin, T. Brauers, J. Stutz and B. J. Finlayson-Pitts, *J. Phys. Chem. A*, 2000, **104**, 1692-1699.
5. Q. Zhang, P. Yin, J. Zhang and J. M. Shreeve, *Chem. Eur. J.*, 2014, **20**, 6909-6914.
6. K. Fujioka, R. I. Kaiser and R. Sun, *J. Phys. Chem. A*, 2023, **127**, 913-923.
7. M. M. Francl, W. J. Pietro, W. J. Hehre, J. S. Binkley, M. S. Gordon, D. J. DeFrees and J. A. Pople, *J. Chem. Phys.* , 1982, **77**, 3654-3665.
8. C. Lee, W. Yang and R. G. Parr, *Phys. Rev. B*, 1988, **37**, 785-789.
9. J. Mikosch, J. Zhang, S. Trippel, C. Eichhorn, R. Otto, R. Sun, W. A. de Jong, M. Weidemüller, W. L. Hase and R. Wester, *J. Am. Chem. Soc.*, 2013, **135**, 4250-4259.
10. T. H. Dunning, Jr., *J. Chem. Phys.*, 1989, **90**, 1007-1023.
11. K. Raghavachari, G. W. Trucks, J. A. Pople and M. Head-Gordon, *Chem. Phys. Lett.*, 1989, **157**, 479-483.
12. K. Fukui, *J. Phys. Chem.*, 1970, **74**, 4161-4163.
13. C. Gonzalez and H. B. Schlegel, *J. Phys. Chem.*, 1990, **94**, 5523-5527.
14. M. Valiev, E. J. Bylaska, N. Govind, K. Kowalski, T. P. Straatsma, H. J. J. Van Dam, D. Wang, J. Nieplocha, E. Apra, T. L. Windus and W. A. de Jong, *Comput. Phys. Commun.*, 2010, **181**, 1477-1489.
15. A. Fried and C. W. Mathews, *Chem. Phys. Lett.*, 1977, **52**, 363-367.
16. J. W. C. Johns, *Can. J. Phys.*, 1961, **39**, 1738-1768.
17. G. Herzberg. K. P. Huber, Molecular Spectra and Molecular Structure: IV. Constants of Diatomic Molecules (Eds.: K. P. Huber, G. Herzberg), Springer US, Boston, MA, 1979..
18. A. Kramida, Y. Ralchenko, J. Reader, and NIST ASD Team (2022). NIST Atomic Spectra Database (version 5.10), *National Institute of Standards and Technology, Gaithersburg, MD.*
19. I. Antonov, A. Chyba, S. D. Perera, A. M. Turner, M. L. Pantoya, M. T. Finn, A. Epshteyn and R. I. Kaiser, *J. Phys. Chem. Lett.*, 2022, **13**, 9777-9785.